ELSEVIER Journal of Materials Processing Technology 50 (1995) 17–38

Journal of Materials Processing Technology

NUMISTAMP: a research project for assessment of finite-element models for stamping processes

E. Oñate*, J. Rojek[1], C. García Garino

International Center for Numerical Methods in Engineering, Univ. Politécnica de Cataluña, Gran Capitán s/n, 08034 Barcelona, Spain

Industrial Summary

This paper describes the objectives and current status of the research project NUMISTAMP currently under development at the International Center for Numerical Methods in Engineering of (CIMNE) located in Barcelona, Spain. The aim of this project is the *assesment* of different finite element models for simulation of sheet stamping processes. The models currently analyzed include: quasistatic viscoplastic flow and elastoplastic solid models and explicit dynamic models. Both shell and continuum elements are considered in most of these cases. The paper presents an overview of the basic features of the different models. Examples of application including some benchmark test cases proposed at NUMISHEET are also presented.

1. Introduction

Considerable effort has been made in recent years in the development of numerical models for analysis of sheet stamping processes. The intrinsic complexity of these problems due to material and geometrical nonlinearities, contact and friction effects and time changing boundary conditions, has made difficult the development of reliable and efficient numerical procedures which allow the solution of practical industrial stamping problems at reasonable times and cost.

Different finite element based codes for sheet-forming analysis have been developed worldwide and many are now operational for the solution of practical sheet-stamping problems. The dispersion in the basic approaches, constitutive equations, finite-element models, solution strategies, etc. chosen for each of these codes is enormous. This adds an extra difficulty for the non-experienced user who is typically confronted with the need to choose a particular code without sufficient knowledge of the

* Corresponding author.

[1] Visiting scientist on leave from Institute of Fundamental Technological Research of Polish Academy of Sciences in Warsaw.

SSDI 0924-0136(94)01367-A

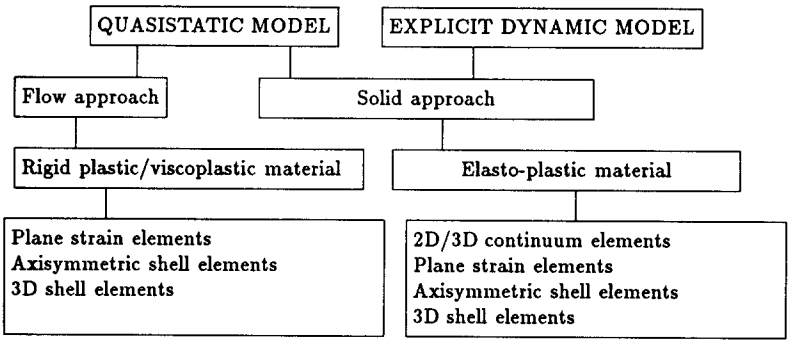

Fig. 1. Different finite element models analyzed in NUMISTAMP project.

advantages and disadvantages of the proposed methodology versus another options available. The need for code bench-marking is obvious and here the success of different initiatives of this kind [1–3] point out a direction to be followed in the near future.

All these facts have motivated the International Center for Numerical Method in Engineering of Barcelona to launch the research project NUMISTAMP. The final goal of this project is to assess, through adequate benchmarking, the performance of finite element models based in different solution methods (quasistatic or explicit dynamic), different kinematic approaches (flow and solid approaches), different constitutive models (rigid–plastic, elasto-plastic, etc.) and different element types (axisymmetric/3D shell elements, 2D/3D continuum elements, etc.). Aspects such as robustness, reliability, accuracy and cost-efficiency of each of the finite-element models chosen will be assessed in detail for different sequential and parallel computer architectures.

The different finite-element models currently under study in project NUMISTAMP are the following:

1. *Quasistatic rigid–plastic/viscoplastic flow model* using plane strain, axisymmetric and 3D shell elements.
2. *Quasistatic elasto-plastic solid model* using 2D/3D continuum elements, as well as plane-strain, axisymmetric shell and 3D shell elements.
3. *Explicit dynamic elasto-plastic solid model* using 2D/3D continuum elements as well as plane-strain, axisymmetric shell and 3D shell elements.

A flow chart showing the different models, currently studied, can be seen in Fig. 1. A brief description of the basic features of each of these models is presented next.

2. Quasistatic flow model

2.1. Basic equations

This approach is typical of fluid mechanics, where a fixed Eulerian frame defining a control volume through which the material flows is used. This method appears to be

more natural for bulk-forming problems such as mould filling, rolling, extrusion, etc. [4]. However, it can be applied also to stamping problems in a straight-forward manner simply by identifying the control volume with the sheet geometry at each deforming step [5–8].

The main variables of the flow approach are the *velocities* $\dot{\boldsymbol{u}}$ of the points of the deforming sheet, and these being linearly related to the rates of deformation $\dot{\boldsymbol{\varepsilon}}$ by

$$\dot{\boldsymbol{\varepsilon}} = \boldsymbol{L}\dot{\boldsymbol{u}}, \tag{1}$$

where $\boldsymbol{L}$ is the standard strain rate operator, i.e. for 2D problems

$$\boldsymbol{L} = \begin{bmatrix} \dfrac{\partial}{\partial x} & 0 \\ 0 & \dfrac{\partial}{\partial y} \\ \dfrac{\partial}{\partial y} & \dfrac{\partial}{\partial x} \end{bmatrix}. \tag{2}$$

The constitutive equation for the flow approach is usually written in the form

$$\boldsymbol{\sigma} = \boldsymbol{D}\dot{\boldsymbol{\varepsilon}}. \tag{3}$$

Eq. (3) is typical of fluid mechanics where $\boldsymbol{\sigma}$ is the Cauchy stress vector and $\boldsymbol{D}$ is the constitutive matrix depending on the flow viscosity only.

It can be shown that Eq. (1) is readily obtained for rigid–plastic/viscoplastic materials. In the isotropic case matrix $\boldsymbol{D}$ is a function of a single nonlinear flow viscosity parameter μ, given for a rigid–plastic Von-Mises material by [5,7,8,4]

$$\mu = \frac{\sigma_y}{3\dot{\bar{\varepsilon}}}, \tag{4}$$

where σ_y is the Von-Mises yield stress and $\dot{\bar{\varepsilon}} = (\frac{2}{3}\dot{\varepsilon}_{ij}\dot{\varepsilon})^{1/2}$. The expression of μ for viscoplastic materials including the effect of microscopic voids can be found in [9,10]. Also note that a cut-off value of μ must be used in quasi-rigid zones where $\dot{\bar{\varepsilon}} \simeq 0$ to prevent singularity.

The set of equations for the flow approach is completed by the rate of virtual work equation written as

$$\int_V \delta\dot{\boldsymbol{\varepsilon}}^{\mathrm{T}}\boldsymbol{\sigma}\,\mathrm{d}V = \int_V \delta\dot{\boldsymbol{u}}^{\mathrm{T}}\boldsymbol{b}\,\mathrm{d}V + \int_\Gamma \delta\dot{\boldsymbol{u}}^{\mathrm{T}}\boldsymbol{t}\,\mathrm{d}\Gamma, \tag{5}$$

where $\boldsymbol{b}$ and $\boldsymbol{t}$ are body forces and surface tractions acting on the sheet volume V and the surface Γ, respectively.

2.2. Finite-element discretization

The form of the constitutive equation (4) for Von-Mises metals defines an *incompressible flow* problem (i.e. $\dot{\varepsilon}_{ii} = 0$). This introduces serious difficulties if the finite-element solution is based on "continuum" elements. However, the incompressibility

condition can be simply imposed in "shell type" elements by setting Poisson's ratio equal to 0.5 and then updating the element thickness making use of the plane stress condition.

It is interesting to note that the overall equations of the flow approach as written in (1)–(5) are analogous to those of standard infinitesimal (incompressible) elasticity [5–8, 4]. This analogy can be exploited to simplify further the computational procedure by directly using standard finite-element codes written for the elasticity case simply replacing displacements and strains by velocities and strain rates, respectively, and the shear modulus by the (non-linear) flow viscosity [5–8].

The velocity field is discretized in the standard form

$$\dot{\boldsymbol{u}} = \boldsymbol{N}\dot{\boldsymbol{a}}, \tag{6}$$

where $\boldsymbol{N}$ and $\dot{\boldsymbol{a}}$ are the shape function matrix and the nodal velocity vector [11].

Some of the elements used currently in the context of the flow approach include:

Plane strain bending element: Two node linear elements based on Timoshenko's beam theory have been chosen [11]. This element simplifies in an easy manner to a two node membrane element.

Axisymmetric shell element: Two node linear axisymmetric shell element based on Reissner–Mindlin axisymmetric shell theory have been selected [5–11]. Again this element simplifies easily to the standard two node axisymmetric membrane element.

3D shell elements: Different thin shell elements based on facet shell theory are used [11]. These include the simple DKT and Morley triangles [11] as well as a new three node bending element with only translational degrees of freedom recently developed by Oñate et al. [12, 25]. Both full bending and membrane cases are considered.

The resulting non linear equilibrium equation can be written after discretization in the form [11]

$$\boldsymbol{r}(\dot{\boldsymbol{a}}, \boldsymbol{x}, t) = \boldsymbol{p}(\dot{\boldsymbol{a}}, t) - \boldsymbol{f}(t, \boldsymbol{x}) = \boldsymbol{0}, \tag{7}$$

where $\boldsymbol{r}, \boldsymbol{p}$ and $\boldsymbol{f}$ stand for the vectors of residual forces, internal forces and external forces, respectively, $\boldsymbol{x}$ is the cartesian coordinate vector and t is the time. Vector $\boldsymbol{p}$ can be written in the flow approach as

$$\boldsymbol{p} = \boldsymbol{K}\dot{\boldsymbol{a}} \quad \text{with} \quad \boldsymbol{K} = \int_V \boldsymbol{B}^{\mathrm{T}} \boldsymbol{D} \boldsymbol{B} \, \mathrm{d}V. \tag{8}$$

In (8) $\boldsymbol{K}$ is the stiffness matrix obtained in terms of the constitutive matrix of Eq. (3) and the strain rate matrix $\boldsymbol{B} = \boldsymbol{L}\boldsymbol{N}$ [5–8].

Eq. (7) can be iteratively solved for the values of $\dot{\boldsymbol{a}}$. For the kth iteration we have

$$\Delta \boldsymbol{a}^k = -[{}^{t+\Delta t}\boldsymbol{H}^k]^{-1} \, {}^{t+\Delta t}\boldsymbol{r}^k, \tag{9}$$

where $\boldsymbol{H}$ is an adequate iteration matrix. Vector $\dot{\boldsymbol{a}}$ is subsequently updated as

$${}^{t+\Delta t}\boldsymbol{a}^{k+1} = {}^{t+\Delta t}\boldsymbol{a}^k + \Delta \boldsymbol{a}^k. \tag{10}$$

The next step is to compute the new stress field by use of Eq. (3). Then the sheet geometry and mechanical properties are updated and the sheet–tool contact and friction conditions are checked. The process is restarted and continues until convergence is achieved. The authors have found that a convergence norm based on the velocities is more appropiate than one based on residual forces. This is due to the cut-off value for the viscosity in quasi-rigid body zones, which can lead to inaccurated stress values in these regions.

Details on the choice of the iteration matrix $\boldsymbol{H}$ and on the different geometry updating procedures available can be found in Refs. [6–8].

2.3. Treatment of frictional contact

The interaction between the sheet and rigid tool surfaces can be treated as a problem of unilaterial frictional contact. The contact surfaces are approximated by a collection of polygons (triangles or quadrilaterals) for 3-D problems and line segments for 2-D problems. The tool surfaces are treated as master surfaces and shell surfaces are treated as slave ones. The contact conditions are considered nodally. A gap/penetration function g is defined for each slave node $\boldsymbol{x}^{(s)}$ as $g(\boldsymbol{x}^{(s)}) = (\boldsymbol{x}^{(s)} - \bar{\boldsymbol{x}}^{(m)}) \cdot \boldsymbol{n}(\bar{\boldsymbol{x}}^{(m)})$, where $\bar{\boldsymbol{x}}^{(m)}$ is the closest point projection of the slave node on the master surface and $\boldsymbol{n}$ is the unit vector, normal to the master surface defined at the point $\bar{\boldsymbol{x}}^{(m)}$ and directed outwards. Contact routines carry out two tasks – searching of the nodes being in contact and computation of contact forces [16, 18].

In the contact searching step the contacting master segment is located for all the slave nodes and the impenetrability condition ($g \geqslant 0$) is checked. Master segments surrounding the closest master node and the segments in the neighbourhood are considered as the potential contacting segments. The time factor is very important in the evaluation of contact searching routines. The searching procedure must find the closest master point with relatively small computational cost. In the algorithm implemented the closest master point is searched in the topological neighbourhood of the previous closest point. The algorithm has found to be quite effective – the contact operations have usually been kept within 10–15% of the total computation time.

The penalty method has been adopted to enforce the normal contact conditions and to compute normal contact forces. It is assumed that the normal contact force $F^{(cn)}$ applied to the slave node is proportional to the amount of penetration ($g < 0$) and a penalty coefficient $k^{(n)}$, *i.e.* $F^{(cn)} = -k^{(n)}g$. The tangential contact forces are computed using the local regularized Coulomb friction law. Elasto-plastic analogy between friction and elasto-plasticity [14, 18] is employed in the friction force calculation. A trial tangential force $\boldsymbol{F}^{(ct)}_{(trial)}$ is calculated as

$$\boldsymbol{F}^{(ct)}_{(trial)} = \boldsymbol{F}^{(ct)}_{(old)} - k^{(t)}\Delta\boldsymbol{u}^{(slip)} \tag{11}$$

where $\boldsymbol{F}^{(ct)}_{(old)}$ is the friction force from the previous time step, $k^{(t)}$ is the penalty coefficient for tangential forces and $\Delta\boldsymbol{u}^{(slip)}$ is the relative displacement of the slave node with respect to the master surface. The trial force is compared with the limit friction force $F^{(ct)}_{(limit)} = \mu F^{(cn)}$, where μ is the friction coefficient, and an appropriate

value is assigned to the friction force $\boldsymbol{F}^{(ct)}_{(new)}$ according to the following rule:

$$\boldsymbol{F}^{(ct)}_{(new)} = \begin{cases} \boldsymbol{F}^{(ct)}_{(trial)} & \text{if } \|\boldsymbol{F}^{(ct)}_{(trial)}\| \leqslant F^{(ct)}_{(limit)}, \\ \boldsymbol{F}^{(ct)}_{(trial)} F^{(ct)}_{(limit)} / \|\boldsymbol{F}^{(ct)}_{(trial)}\| & \text{if } \|\boldsymbol{F}^{(ct)}_{(trial)}\| > F^{(ct)}_{(limit)}. \end{cases} \tag{12}$$

2.4. Prediction of spring-back effects

The computation of spring-back effects is of importance in sheet stamping operations. In principle only finite element computations incorporating elastic effects in the constitutive equations (i.e. elastoplastic or elasto-viscoplastic models) can deal with elastic recovery effects in a straight forward manner.

The authors have investigated the possibility of predicting spring-back effects using a rigid-plastic/viscoplastic flow formulation with the following procedure:

(i) During the loading process the effects of elasticity effects are neglected in all elements and the flow formulation as previously described is used.

(ii) Once the tools are removed all elements are assumed to behave elastically. This simply implies replacing the original constitutive matrix $\boldsymbol{D}(\mu)$ by that of standard elasticity $\boldsymbol{D}(E, \nu)$ where E is Young's modulus and ν is Poisson's ratio.

(iii) Equilibrium under the initial stress field is obtained by using an updated Lagrangian iterative approach accounting for geometrically nonlinear effects. The simplest iteration process can be written in the form

$$\begin{aligned} \Delta \boldsymbol{a}^k &= -\boldsymbol{K}^{-1} \int_V [\boldsymbol{B}^k]^{\mathrm{T}} \boldsymbol{\sigma}^k \, \mathrm{d}V, \\ \boldsymbol{a}^{k+1} &= \boldsymbol{a}^k + \Delta \boldsymbol{a}^k, \\ \boldsymbol{\sigma}^{k+1} &= \boldsymbol{\sigma}^k + \boldsymbol{D}\boldsymbol{B}^k \Delta \boldsymbol{a}^k, \end{aligned} \tag{13}$$

where $\boldsymbol{\sigma}^0$ are the initial stresses in the last increment during the stamping process using the flow approach, $\boldsymbol{K}$ is the elastic stiffness matrix kept constant during the iterations and $\boldsymbol{B}^k$ is the standard strain matrix from small displacement theory which is updated for each iteration. The iterative process stops when the residual forces equal to $-\int \boldsymbol{B}^{\mathrm{T}} \boldsymbol{\sigma} \, \mathrm{d}V$ satisfy a prescribed norm. This process can be enhanced by scaling the initial stresses which are then applied in an incremental manner.

3. Quasistatic solid model

3.1. Basic concepts

This approach uses a total or updated description of the motion. The basic variables are the displacements, $\boldsymbol{u}$, of the deforming sheet points and these are related to the strains, $\boldsymbol{\varepsilon}$, by standard non-linear kinematic expressions of the form

$$\boldsymbol{\varepsilon} = (\boldsymbol{L} + \bar{\boldsymbol{L}}(\boldsymbol{u}))\boldsymbol{u}, \tag{14}$$

where $\boldsymbol{L}$ is the linear operator of Eq. (1) and $\bar{\boldsymbol{L}}(\boldsymbol{u})$ is a nonlinear strain operator accounting for large displacement effects [11]. On the other hand, the constitutive equations relating the appropiate stress measures, $\boldsymbol{\sigma}$, and the strains $\boldsymbol{\varepsilon}$ must be written in an objective manner accounting for large strain effects. In our work the elasto-plastic model has been chosen. Here two major branches can be recognized: hypoelastic and hyperelastic models. Hypoelastic models have been traditionally used for the constitutive description of large strain elasto-plasticity [16]. It is the experience of the authors [20–22] that hyperelastic models have a big potential for the kind of material nonlinearities appearing in metal forming problems and they have been chosen for this work.

3.2. Kinematics description

A standard multiplicative kinematic approach has been chosen. Thus, the deformation gradient is expressed in terms of the elastic and plastic counterparts as

$$\boldsymbol{F} = \boldsymbol{F}^{\mathrm{e}}\boldsymbol{F}^{\mathrm{p}}. \tag{15}$$

Eq. (15) leads to the standard additive form of the rate of deformation tensor $\boldsymbol{d}$ into an elastic and a plastic part [20–22].

3.3. Constitutive expressions

The constitutive response of the hyperelastic model chosen is established in the context of irreversible thermodynamics. Taking into account *objectivity* and *material symmetry* [20] the free energy function can be written as

$$\bar{\psi} = \psi^{\mathrm{e}}(\boldsymbol{e}^{\mathrm{e}}) + \psi^{\mathrm{p}}(\boldsymbol{q}), \tag{16}$$

where $\boldsymbol{e}^{\mathrm{e}}$ are the elastic Almansi strains in the current configuration and $\boldsymbol{q}$ is a set of internal variables also defined in the current configuration.

The following yield criterion is introduced:

$$f = f(\boldsymbol{e}^{\mathrm{e}}, \boldsymbol{q}). \tag{17}$$

For the sake of simplicity an associated flow rule is considered. The model is completed with the additive decomposition $\boldsymbol{d} = \boldsymbol{d}^{\mathrm{e}} + \boldsymbol{d}^{\mathrm{p}}$ and with Clasius–Duhem inequality written as $-\rho\dot{\psi} + \boldsymbol{\sigma}\colon \boldsymbol{d} \geqslant 0$. This leads to the following expressions for the stresses $\boldsymbol{\sigma}$ and the plastic dissipation γ:

$$\sigma = \rho\frac{\partial\psi(\boldsymbol{e}^{\mathrm{e}})}{\partial\boldsymbol{e}^{\mathrm{e}}}, \qquad \gamma = \boldsymbol{\sigma}\colon \boldsymbol{d}^{\mathrm{p}} - \rho\frac{\partial\psi^{\mathrm{p}}}{\partial\boldsymbol{p}}\colon \dot{\boldsymbol{q}} \geqslant 0. \tag{18}$$

From this the spatial elasticity tangent tensor is found as

$$\boldsymbol{D}^{\mathrm{e}} = \frac{\partial\psi(\boldsymbol{e}^{\mathrm{e}})}{\partial\boldsymbol{e}^{\mathrm{e}} \otimes \partial\boldsymbol{e}^{\mathrm{e}}}. \tag{19}$$

Finally, the elastoplastic constitutive law is written as

$$\overset{\circ}{\boldsymbol{\sigma}} = \boldsymbol{D}^{ep} : \boldsymbol{d} \quad \text{with} \quad \boldsymbol{D}^{ep} = \boldsymbol{D}^{e} - \frac{\left\{\dfrac{\partial f}{\partial \boldsymbol{\sigma}} : \boldsymbol{D}^{e}\right\} \otimes \left\{\boldsymbol{D}^{e} : \dfrac{\partial f}{\partial \boldsymbol{\sigma}}\right\}}{\dfrac{\partial f}{\partial \boldsymbol{\sigma}} : \boldsymbol{D}^{e} : \dfrac{\partial f}{\partial \boldsymbol{\sigma}} + H}, \tag{20}$$

where $\overset{\circ}{\boldsymbol{\sigma}}$ is the Truesdell stress rate, $\boldsymbol{D}^{ep}$ is the elastoplastic spatial tangent tensor and H is the hardening coefficient.

Further details of the theoretical aspects of this model can be found in Refs. [20–22].

3.4. Finite elements chosen and numerical implementation of the model

Both continuum and shell elements have been implemented using the hyperelastic model above described.

Continuum elements chosen for 2D and 3D applications are the four noded quadrilateral and the eight noded hexahedral, respectively [11]. Plastic incompressibility constraints have been dealt with using a mixed element based on a quadrilateral element with constant pressure (Q4/PO) [20]. One of the main advantages of continuum elements is that they allow the treatment of two-face contact conditions. The price paid is the request for a thickness discretization although a single element across the thickness can be successfully used in many occasions.

Shell elements chosen are based on the non-linear shell theory developed by Simo and co-workers [23, 24]. New triangular and quadrilateral shell elements which show a promising behaviour for sheet metal forming analysis have been derived by the authors and the reader is addressed to Ref. [25] for details.

The numerical solution of the elastoplastic problem is based on a Newton–Raphson algorithm combined with an elastic predictor-plastic corrector scheme. Full details of this approach can be found in [20–22].

Frictional contact effects are treated as described in Section 2.3 for the flow approach but using in this case a Quasi-Coulomb Law [20].

Spring-back effects are modelled in a natural manner in this formulation since the effect of elasticity is included throughout the process.

4. Explicit dynamic model

Explicit dynamic methods have recently become very popular in the context of the solid approach, as they do not require the solution of a system of equations. The basic idea is the solution of the dynamic equilibrium equation at time t using an explicit integration scheme with a diagonal matrix. The explicit–dynamic algorithm is shown in Box 1. The advantage of this procedure is that the stiffness matrix does not need to be formed and that contact conditions are modelled accurately in a simple manner because of the requirements of small time steps: moreover they can be easily parallelized.

Explicit Dynamic Solution

Discretized dynamic equilibrium equation

$$\boldsymbol{M}\ddot{\boldsymbol{u}} + \boldsymbol{p}(\boldsymbol{u}) = \boldsymbol{f}$$

Solution at time t_n

1) $\ddot{\boldsymbol{u}}^n = \boldsymbol{M}_D^{-1}[\boldsymbol{f}^n - \boldsymbol{p}^n]; \quad \boldsymbol{M}_D = \text{diag}\,\boldsymbol{M}$
2) $\dot{\boldsymbol{u}}^{n+1/2} = \dot{\boldsymbol{u}}^{n-1/2} + \frac{1}{2}\ddot{\boldsymbol{u}}^n(\Delta t^{n-1} + \Delta t^n)$
3) $\boldsymbol{u}^{n+1} = \boldsymbol{u}^n + \Delta t^n \dot{\boldsymbol{u}}^{n+1/2}$
4) Compute strains and stresses
5) Compute $\boldsymbol{f}^{n+1}, \boldsymbol{p}^{n+1}$
6) Check frictional contact conditions
7) New solution at time t_{n+1}

Box 1. Flow chart of explicit dynamic solution for the solid approach.

Both the continuum and shell elements described in previous section have been implemented also in the context of the explicit–dynamic model. The constitutive model used is the previously described in Sections 3.2 and 3.3. Continuum elements require much smaller time steps than do shell type elements, as the time increment is inversely proportional to the thickness stiffness. Greater time steps can be used in the shell case if the rotational inertia terms are scaled to figures closed to the translational values.

Once the final deformation of the sheet is obtained the dynamic analysis can be continued with removed contact conditions to obtain the deformed shape after springback. The springback analysis is thus a problem of free vibrations. Introducing an adequate structural damping leads to an equilibrium state giving the deformed shape after springback. The final state can be regarded as steady when the vibrations in the lowest structural mode are damped out. The damping used in our analysis was proportional to the mass matrix, i.e. $\boldsymbol{C} = \alpha \boldsymbol{M}$. The critical damping for the lowest vibration mode was estimated using the following formula derived from the analytical solution of damped vibration problem

$$\alpha = \frac{2}{t^{(r)}} \ln f, \tag{21}$$

where $t^{(r)}$ is the user specified time (greater than the natural period) allowing to diminish the energy of damped vibrations to the required fraction f of the non-damped value; $f = 0.01$ was usually taken in our analyses.

Experience proves that the time period required for the springback analysis with the explicit–dynamic code is extremely long, since the critical time step is very small when compared to the period of natural vibrations. More economical solution of the springback problem by switching the explicit analysis to a quasistatic implicit one is currently being implemented in the explicit code STAMPACK developed by the authors group.

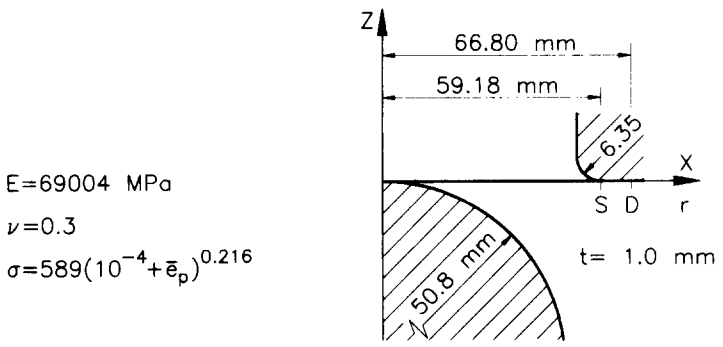

Fig. 2. OSU problem: Geometry and material data.

The explicit dynamic solution in the context of the flow approach is not so attractive, since a nonlinear equation system must be solved for each time step. Further details can be found in [8].

5. Examples

5.1. Hemispherical punch stretching

The first example corresponds to the well known hemispherical punch stretching test proposed by Ohio State University [1] and has been studied in detail in [20]. The geometry and material properties are shown in Fig. 2. This problem has been analyzed with the following finite element models:

(1) *Quasistatic flow model.* 14 two node axisymmetric shell elements were used. The time increment was taken equal to 0.5 s for a punch speed of 1 mm/s. An average of 3 iterations per time step for convergence using a velocity norm of 10^{-2} were needed in all cases.

(2) *Quasistatic solid model.* A mesh of 14 four node quadrilateral continuum elements with two elements across the thickness was used. The time increments used were equal to 0.7, 0.3 and 0.15 s for friction values of 0.0, 0.15 and 0.30, respectively. Convergence was achieved in an average of 2 iterations per time step in all cases.

(3) *Explicit–dynamic model.* The same discretization as in (2) was taken although a single element across the thickness was chosen in this case. An automatic time increment was used.

Figs. 3, 4 and 5 show the equivalent plastic strain curves obtained with the three models studied for different punch travels of 10, 20, 30 and 40 mm, for the friction coefficients of 0.0, 0.15 and 0.30 respectively. The coincidence of results in all cases is remarkable.

Numerical results were obtained using a Convex C-120 computer. CPU times for the quasistatic flow and solid approaches were approximately the same in both cases

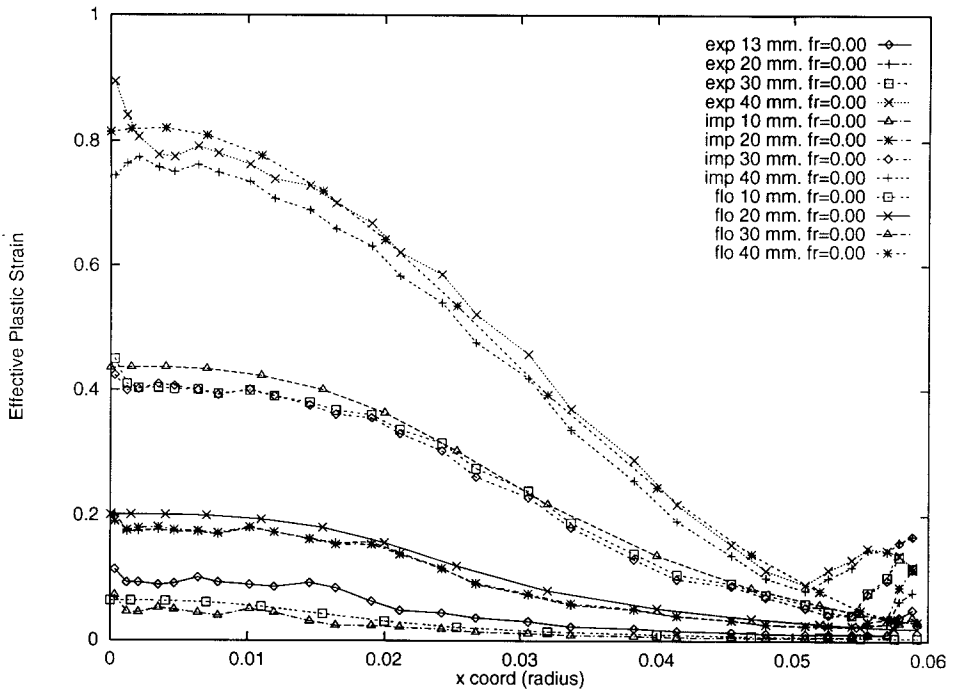

Fig. 3. OSU problem $\mu = 0$: Effective plastic strain profiles for different punch travels: exp, explicit dynamic problem; imp, quasistatic elastoplastic model; flo, quasistatic flow model.

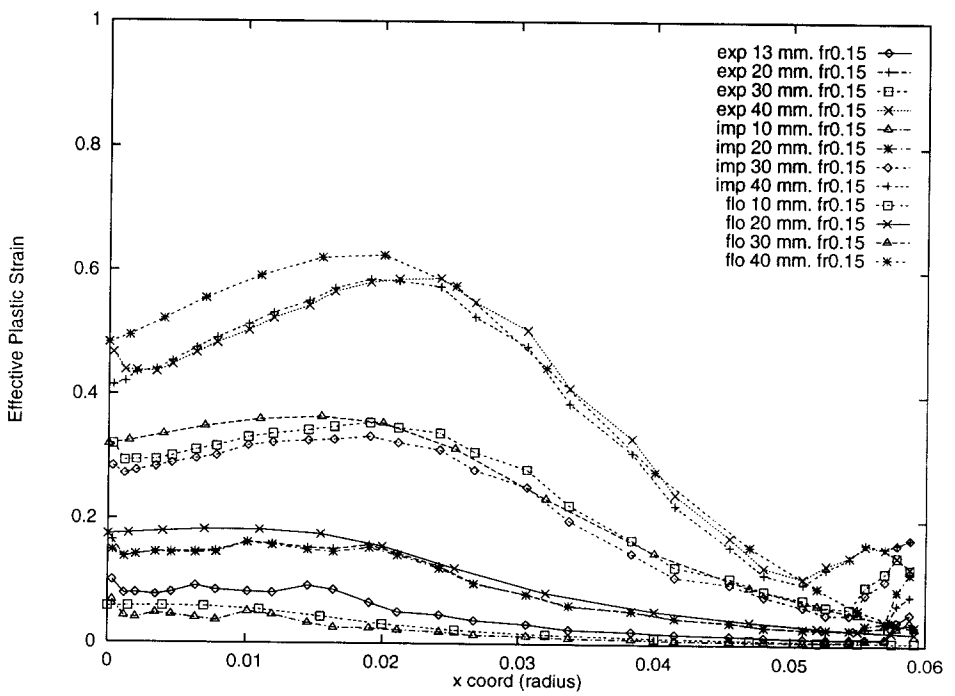

Fig. 4. OSU problem $\mu = 0.15$: Effective plastic strain profiles for different punch travels: exp, explicit dynamic problem; imp, quasistatic elastoplastic model; flo, quasistatic flow model.

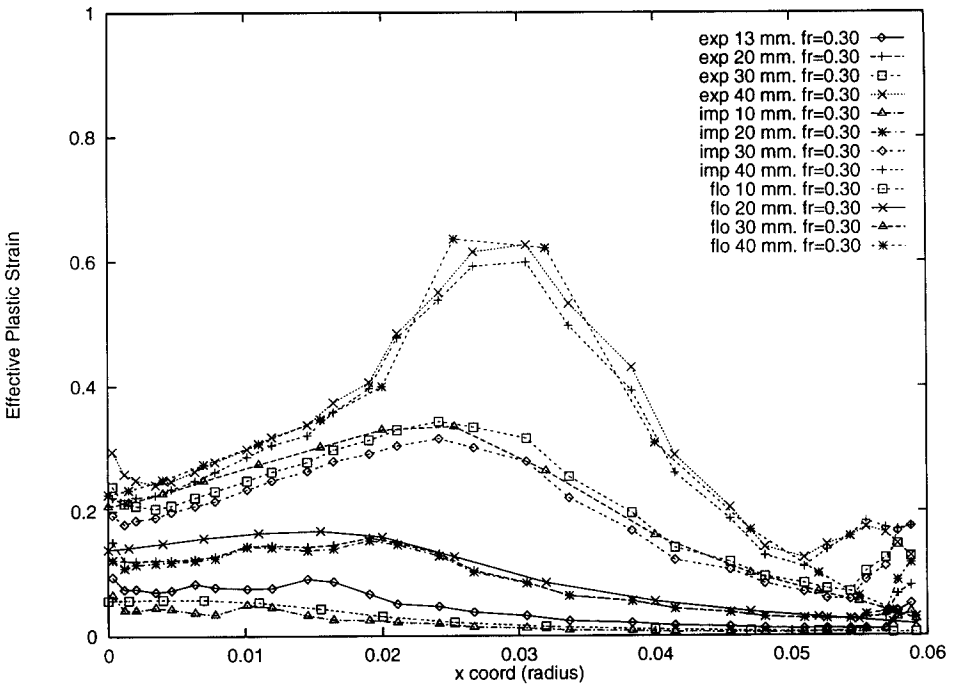

Fig. 5. OSU problem $\mu = 0.30$: Effective plastic strain profiles for different punch travels: exp, explicit dynamic problem; imp, quasistatic elastoplastic model; flo, quasistatic flow model.

and equal to 50, 90 and 180 s for friction values of 0.0, 0.15 and 0.30, respectively. The explicit–dynamic solution took around 400 s in all cases. These differences are to be expected for this simple case where the explicit–dynamic approach is not competitive with the quasistatic codes.

5.2. *Computation of springback effects*

A 2D drawing of a U-profile which was the benchmark example no. 3 in Ref. [2] has been analyzed to test the ability of the different approaches to predict springback effects properly. The geometry of the problem is shown in Fig. 6(a). The case presented here is that of the blank of aluminium alloy and the blankholding forces of $F = 2.45$ and 20 kN. Material properties were the following: $E = 71$ GPa, $\nu = 0.33$, $\rho = 2700\ \text{kg/m}^3$ and $\sigma = 579.79\ (0.01658 + \varepsilon^{(p)})^{0.3593}$ MPa. A friction coefficient $\mu = 0.162$ was used. The explicit–dynamic solution was attempted first. Since the width of the blank, 35 mm, was much greater than its thickness, 0.81 mm, the problem was considered as a plain strain one. Due to the symmetry a half of the blank was modeled with 358 4-node continuum elements using 2 layers of elements through the thickness. The problem was analyzed with the actual mass density and the punch velocity changing harmonically with $v_{\max} = 10$ m/s. The explicit–dynamic analysis

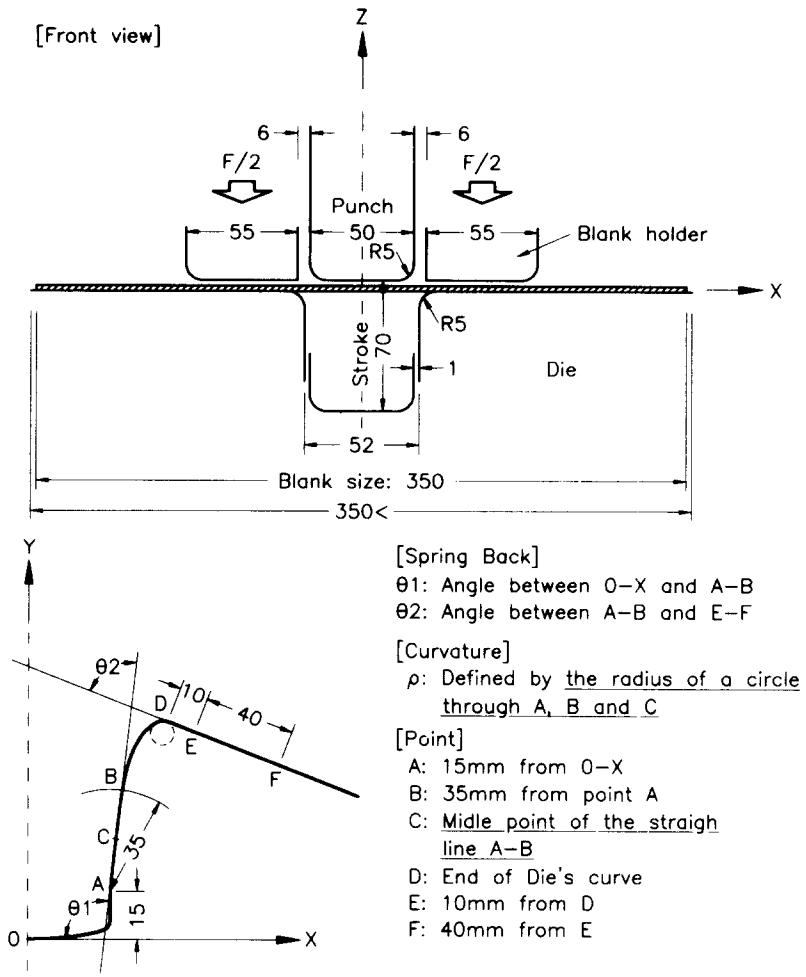

Fig. 6. 2D draw bending: (a) geometry of the problem; (b) measuring method.

with a constant time increment of 5×10^{-8} s took 200 000 steps and 477 min. CPU on a Silicon Graphics – Indigo R400 workstation and the springback analysis – 400 000 steps and 820 min CPU, respectively. The results obtained in the simulation are in very good agreement with the average experimental results given in Ref. [2] (Fig. 7). Springback angles and the radius of curvature of the side wall defined in Fig. 6(b) have the following values: $\theta_1 = 108.9°$, $\theta_2 = 74.3°$ and $\rho = 100.5$ mm for the present simulation and $\theta_1 = 112.4°$, $\theta_2 = 72.8°$, $\rho = 106$ mm for the experiments [2].

The problem was analyzed next using the quasistatic flow model. 90 plane strain shell type elements were used for the analysis. The CPU time required in this case was 340 s, whereas the springback computation took only 12 s. This shows the inefficiency of the explicit–dynamic approach to model springback effects as previously discussed.

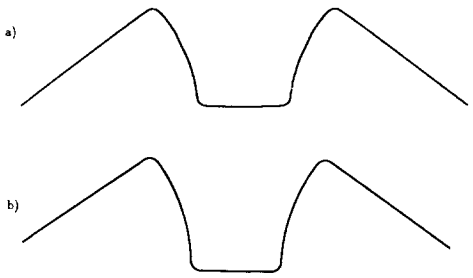

Fig. 7. 2D draw bending – deformed shape after springback: (a) from an experiment; (b) from the numerical simulation using explicit dynamic model.

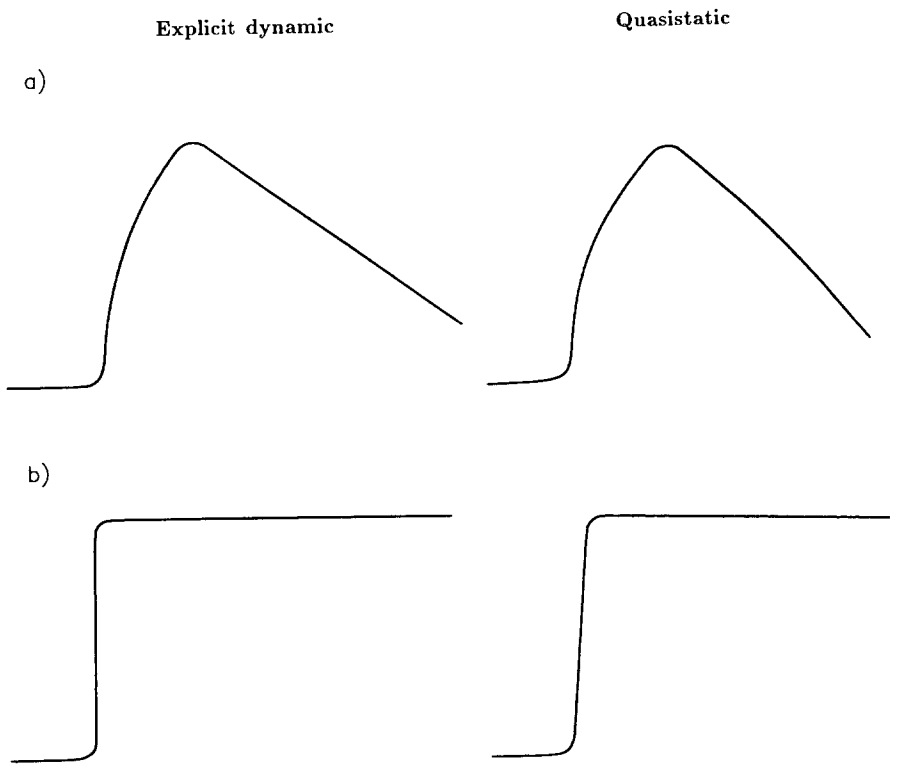

Fig. 8. 2D draw bending – deformed shapes after springback: (a) blankholding force 2.45 kN; (b) blankholding force 20 kN.

Similar results were obtained using the quasistatic solid approach with the same number of elements as for the explicit–dynamic case. The comparison of the deformed shapes after springback for the different models and for both values of the blankholding force is given in Fig. 8.

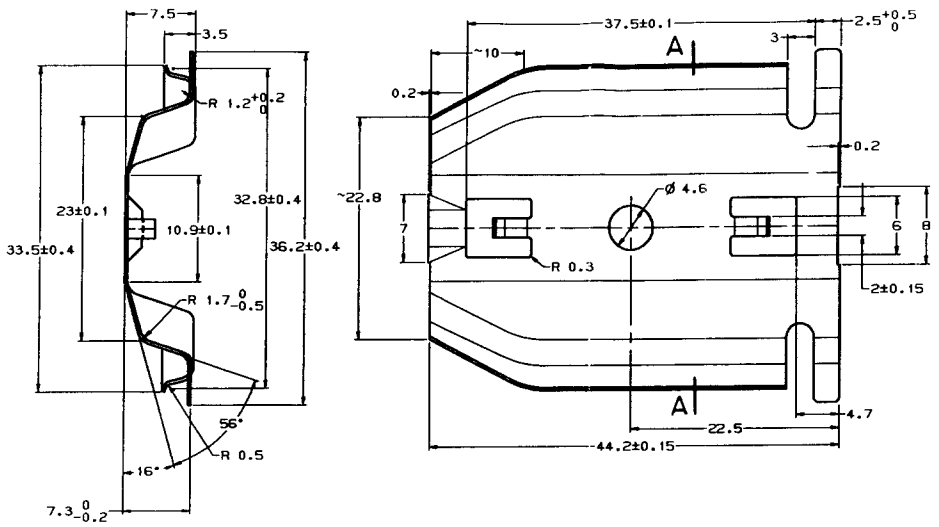

Fig. 9. Forming of the industrial fastener – geometry of the part.

5.3. Sectional analysis

Despite the great development of the hardware and finite element software capabilities, it is still difficult to perform 3-D analysis for sheet parts of complex geometry and simplified 2-D models of 3-D parts are usually considered. A section A-A of an industrial fastener (Fig. 9) was analyzed assuming the plane strain state. The explicit dynamic approach was chosen in this case. The material of the sheet is a stainless steel with $E = 2.1 \times 10^5$ MPa, $\nu = 0.3$; elasto-plastic model with initial yield stress $\sigma^{(Y)} = 850$ MPa and isotropic linear hardening modulus $H = 700$ MPa were assumed. The thickness of the sheet is 0.3 mm. A friction coefficient $\mu = 0.1$ was taken. 200 quadrilateral shell elements with the boundary conditions imposing plane strain state were used to model the cross-section. The tooling consists of the punch and die only. Both the forming process and subsequent springback have been simulated. Different stages of deformation are presented in Fig. 10. The deformed shape at the end of forming and the deformed shape of the profile after springback are compared in Fig. 11.

A section A-A of an automobile part (Fig. 12) was next analyzed using again plane strain conditions. The material is steel with the following parameters: $E = 2.1 \times 10^5$ MPa, $\nu = 0.3$, $\sigma^{(Y)} = 260$ MPa and $H = 9.0$ MPa. The thickness of the sheet is 0.9 mm and the friction coefficient $\mu = 0.1$ was assumed. The strip discretized with 200 quadrilateral shell elements was analyzed again with the explicit–dynamic code STAMPACK. Different stages of the deformation are presented in Fig. 13. The final deformed shape of the strip is shown in Fig. 14(a). In Fig. 14(b) the final profile is compared with the shape after springback.

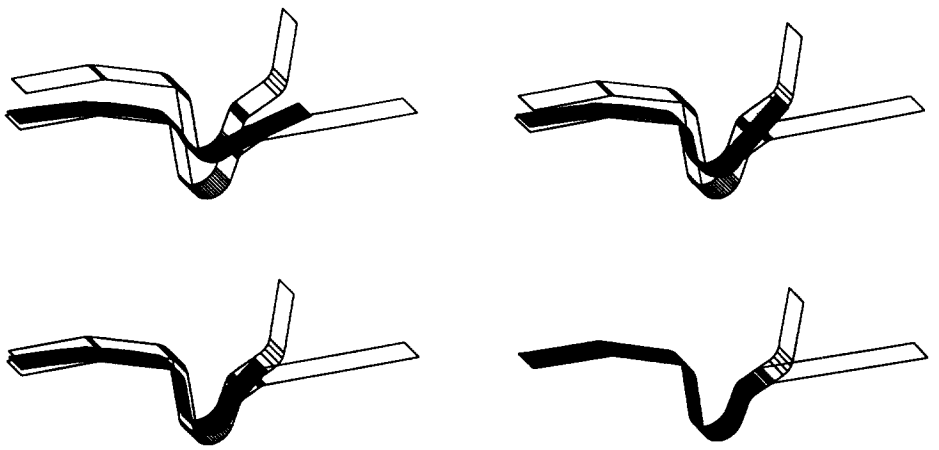

Fig. 10. Forming of the industrial fastener – different stages of the simulation.

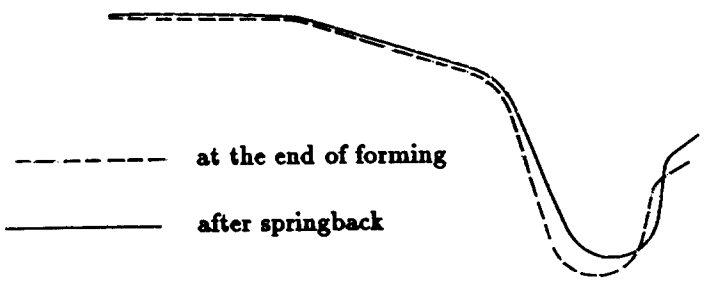

Fig. 11. Forming of the industrial fastener – comparison of the shape at the end of forming with the shape after springback.

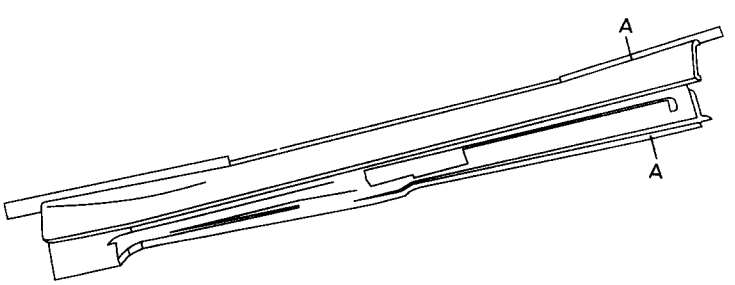

Fig. 12. 3D view of the analyzed part.

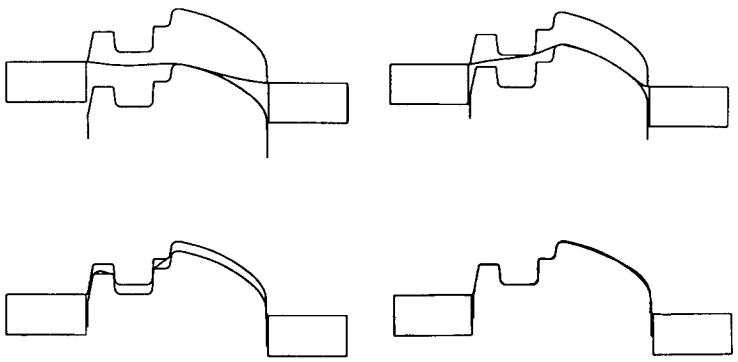

Fig. 13. Sectional analysis – different stages of the simulation.

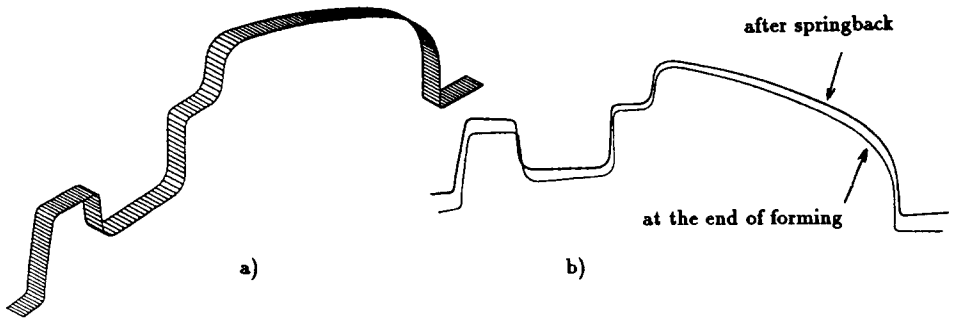

Fig. 14. Results of the sectional analysis: (a) deformed strip; (b) comparison of the deformed shape at the end of forming and after the springback.

5.4. *Analysis of 3D deep drawing problem*

A square cup drawing (Fig. 15), the benchmark problem no. 1 in Ref. [1], was finally analyzed with the explicit–dynamic approach. The material properties are the following: mild steel (thickness 0.78 mm), $E = 2.06 \times 10^5$ MPa, $\nu = 0.3$, $\sigma = 565.32\,(0.007117 + \varepsilon^{(p)})^{0.2589}$ MPa. The friction coefficient was $\mu = 0.162$ and the blankholding force 19.6 kN. A quarter of the problem was discretized with 900 8-node hexahedral solid elements.

The analysis was carried out with the actual mass density and the punch speed changing harmonically with the peak value of 10 m/s. The deformation for the punch stroke of 40 mm was obtained. The simulation was run on a Silicon Graphics – Indigo R400 workstation. It took 22 h 12 min of CPU time and required 72 860 steps with a time increment changing from 1.138×10^{-5} to 7.200×10^{-6} sec.

The deformed square cup shape is shown in Fig. 16(a). The draw-in values obtained, DX and DD as defined in Fig. 16(a) have been compared in Table 1 with other

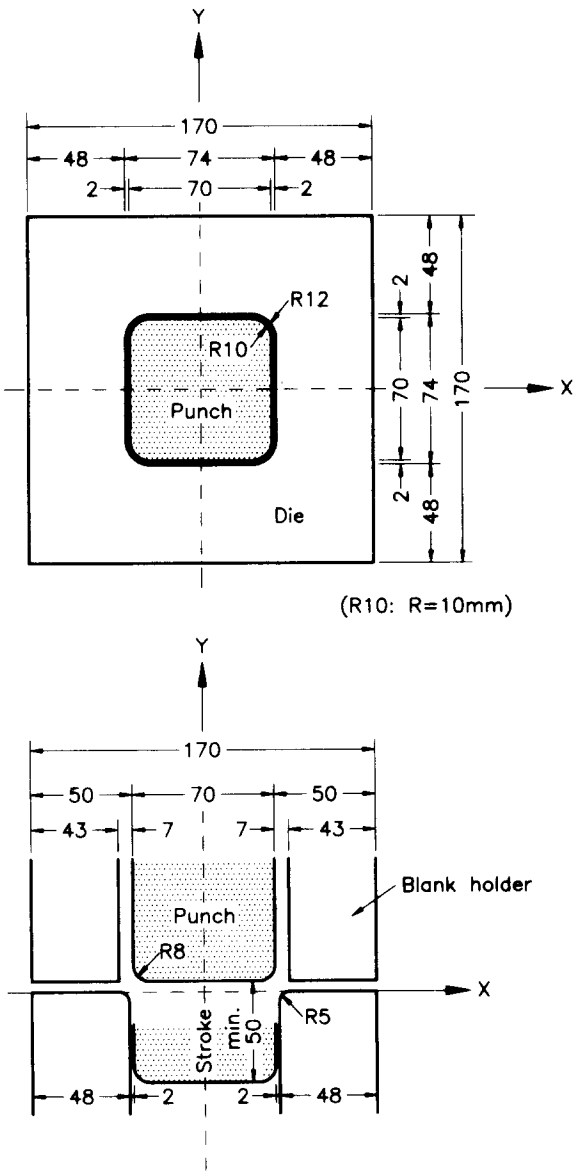

Fig. 15. Geometry of the square cup deep drawing problem.

numerical results and average experimental results reported in Ref. [2]. The amounts of draw-in obtained in our analysis are in agreement with the reference results.

Thickness logarithmic strain contours at punch stroke of 40 mm are presented in Fig. 16(b). In Fig. 17 we have compared our results with other numerical results and average experimental results reported in Ref. [2]. The thickness distribution along lines O–A and O–B (Fig. 16(a)) obtained shows good agreement both with experimental tests and numerical results obtained with other codes. Small discrepancies

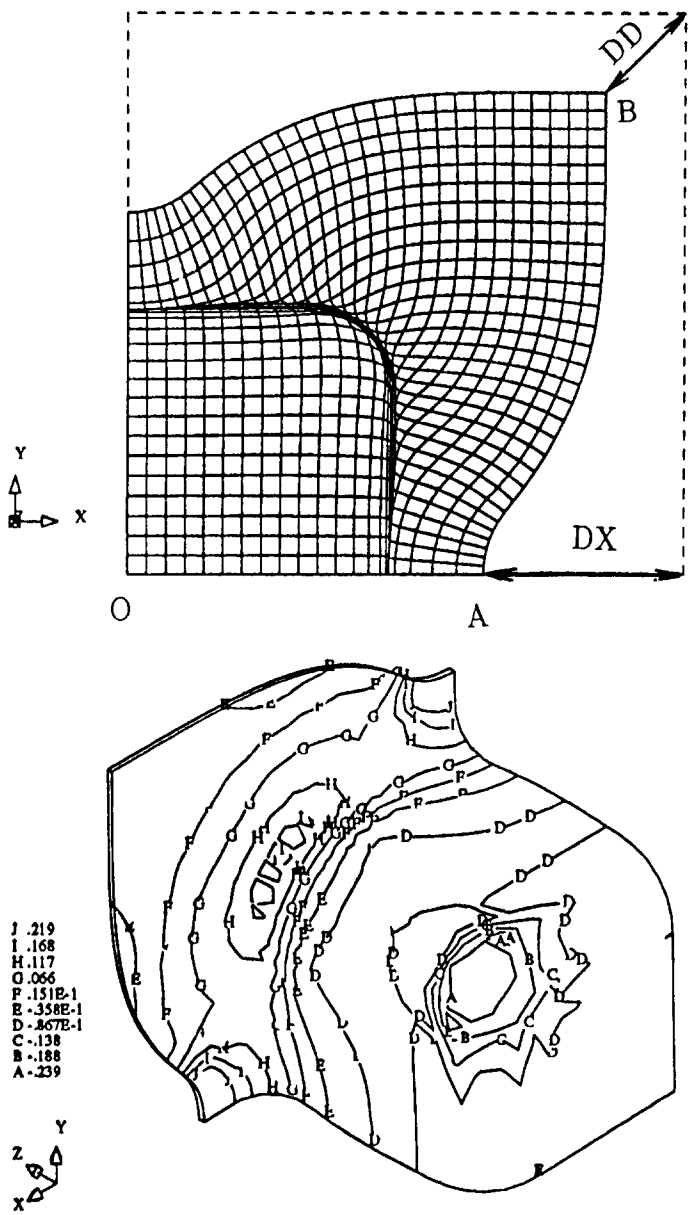

g. 16. Square cup deep drawing: (a) initial and deformed blank outlines; (b) thickness strain contours.

Table 1
Comparison of draw-in values for the benchmark problem [2]

Draw-in	Pres. sim. solid	Numerical B1-Sim-1	Numerical B1-Sim-6	Numerical B1-Sim-25	Experiment average
DX	27.1	28.9	30.03	28.43	27.95
DD	15.3	16.2	16.43	15.46	15.36

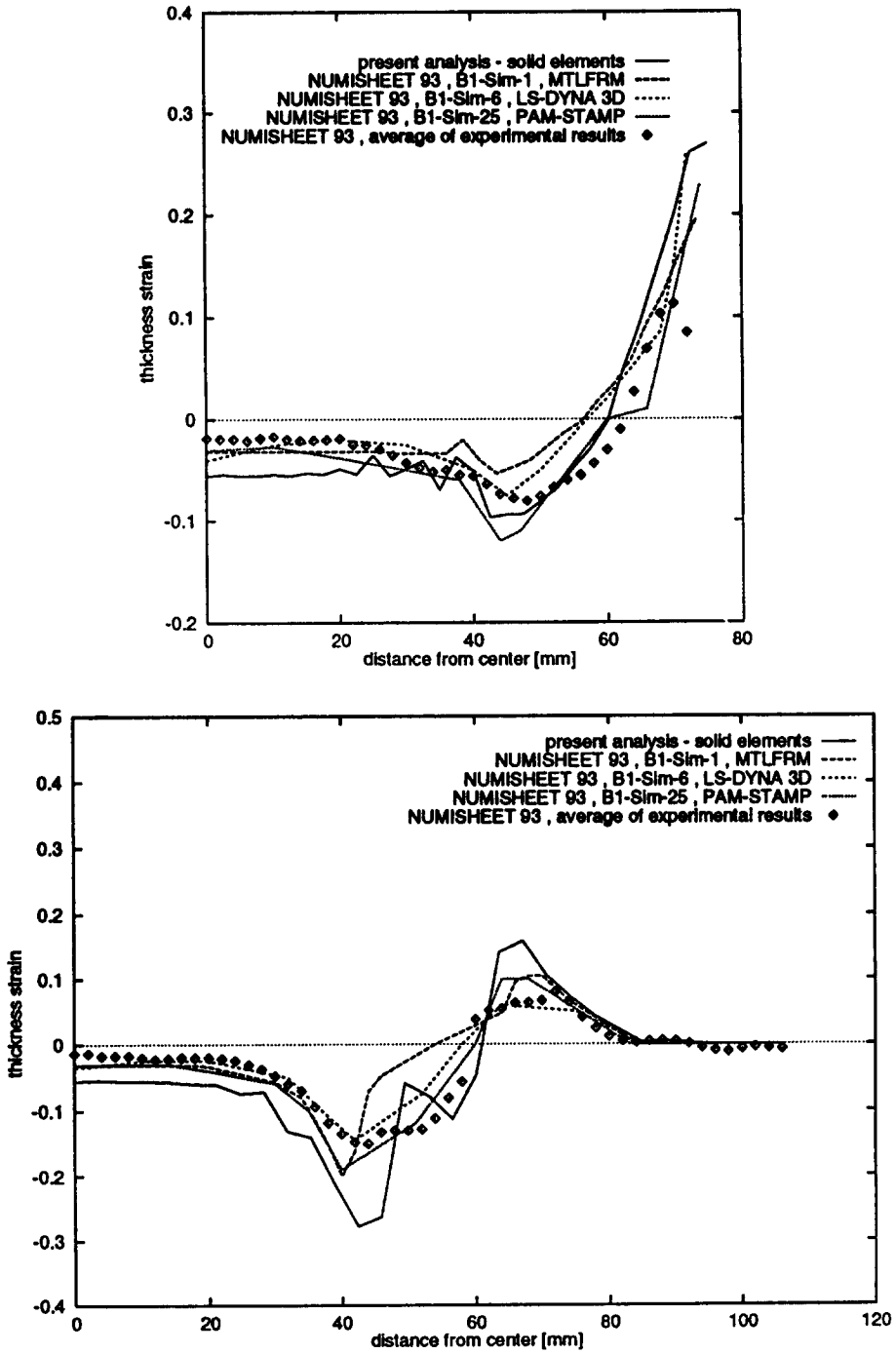

Fig. 17. Thickness strain distribution: (a) along line O–A; (b) along line O–B.

can be explained by the fact that we have used just one element through the thickness and reference results were obtained with shell elements with explicit integration through the thickness.

6. Concluding remarks

This paper reports a first attempt to develop a systematic methodology for evaluating the performance of different finite-element approaches for sheet stamping analysis. Although it was not possible to analyze the test examples chosen with all the different approaches studied some preliminary conclusions can be drawn at this stage.

(1) The three formulations studied (i.e. quasistatic flow and solid approaches and the explicit–dynamic approach) are adequate for analysis of sheet stamping problems giving the same accuracy for the examples studied.

(2) The computer cost of the quasistatic flow and solid approaches was found to be very similar in all cases. On the other hand for small problems the explicit dynamic model with continuum elements required always much larger CPU time. These requirements diminished drastically when shell elements were used.

(3) The explicit dynamic approach does not seems suitable for springback computations since the CPU time requirements are one order of magnitude greater than those needed for the other two approaches.

(4) Despite these drawbacks the small memory requirements of the explicit dynamic approach make this procedure extremely attractive for solving large size stamping problems. Certainly quasistatic models are in clear disadvantage here unless they are combined with iterative type solvers. The comparisons of these two alternatives will be the object of much research in the authors' group in the near future.

Acknowledgements

The authors thank Francisco Zarate for his collaboration concerning some of the simulations in this work. The financial support of CONFOSIM project from Ministerio de Industria of Spain is also gratefully acknowledged. Thanks are also given to the companies Mikalor S.A. and Candemat S.A. for providing data for the examples of Section 5.3.

References

[1] J.K. Lee., R.H. Wagoner and E. Nakamachi., A benchmark test for sheet forming analysis, Ohio State University, July 1990.

[2] A. Makinouchi, Nakamachi, E. Oñate and R. Wagoner (Eds.) *NUMISHEET 2d. Int. Conference on Numerical Simulation of 3-D sheet Metal Forming Processes, Verification of Simulation with Experiment.* 31 August–2 September 1993, Isekava, Japan.

[3] VDI. Finite element simulation of 3D sheet metal forming processes in automotive industry, VDI Berichte 894, Zürich, 1991.

[4] O.C. Zienkiewicz., P.C. Jain and E. Oñate., Flow of solids during forming and extrusion. Some aspects of numerical solutions, *Int. J. Solids Struct.*, 14 (1987) 14–28.
[5] E. Oñate and O.C. Zienkiewicz., A viscous shell formulation for the analysis of thin sheet metal forming, *Int. J. Mech. Sci.*, 25, (1983) 305–335.
[6] E. Oñate, and C. Agelet de Saracibar., Analysis of sheet metal forming problems using a selective bending-membrane formulation, *Int. J. Numer. Eng.*, 30, (1990) 1577–1593.
[7] E. Oñate and C. Agelet de Saracibar., Numerical modelling of sheet metal forming problems, in: P. Hartley, I. Pillinger and C. Sturgess (eds.), *Numerical Modelling of Material Deformation Processes: Research, Developments and Applications*, Springer, Berlin, 1992. pp. 318–354.
[8] E. Oñate and C. Agelet de Saracibar., Alternatives for finite element analysis of sheet metal forming problems, in: J.L. Chenot., R. Wood and Zienkiewicz (Eds.), *NUMIFORM '92*, A.A. Balkema, Rotterdam, Netherlands, 1992, pp. 79–89.
[9] C. Agelet de Saracibar, and E. Oñate., Plasticity for porous metals, in: D.R.J. Owen, E. Hinton and E. Oñate (Eds.), *Proc. 2nd Internat. Conf. on Computational Plasticity*, Pineridge Press, Swansea, (1989), pp. 159–152.
[10] C. Agelet de Saracibar., Finite element analysis of sheet metal forming processes, Ph.D. Thesis., Univ. Politec. Catalunya, Barcelona, (1990) (in Spanish).
[11] O.C. Zienkiewicz and R.L. Taylor., *The Finite Element Method*, 4th ed., Vol. 2, McGraw-Hill, New York, 1991.
[12] E. Oñate., M. Cervera and F. Zarate., A three node triangular shell element with translational degrees of freedom, Research Report CIMNE, Barcelona, 1995.
[13] J.B. Dalin and E. Oñate., An automatic algorithm for contact problems: Applications to sheet metal forming, *Proc. Numiform '89*, A.A. Balkema, 1989, pp. 419–425.
[14] D. Perić and D.R.J. Owen., Computational model for 3D contact problems with friction based on the penalty method, in: N. Bicanic, P. Marovic, D.R.J. Owen, V. Jovic and A. Mihanović (eds.), *Nonlinear Engineering Computations*, Pineridge Press, Swansea, 1991, pp. 121–142.
[15] P. Wriggers., J.C. Simo and R.L. Taylor., Penalty and augmented Lagrangian Formulations for contact problems, *Proc NUMETA '85*, A.A. Balkema, Rotterdam, Netherlands, 1985, 97–106.
[16] A. Heege and P. Alart., On an implicit contact friction algorithm dedicated to 3D sheet forming simulation, in: F.L. Chenot, R. Wood and O.C. Zienkewicz (Eds.), *NUMIFORM '92* A.A Balkema, Rotterdam, Netherlands, 1992.
[17] K. Schweizerhof and J.O. Hallquist., Explicit integration scheme and contact formulations for thin sheet metal forming, *Proc. FE-Simulation of 3-D sheet Metal Forming Processes in Automatic Industry*, VDI, 1991 405–440.
[18] C. Agelet de Saracibar, Numerical simulation of frictional contact problems, *Lectures Notes of the A short Course on Finite Element Procedures for Plsticity and Viscoplasticity*, Barcelona, Spain, 2–3 April, 1992.
[19] T.J.R. Hughes., Numerical implementation of constitutive models: Rate independent deviatoric plasticity, in: Nemat-Nasser et al. (Eds.), *Theoretical Foundation for Large Scale Computations for Non linear Material Behaviour*, Vol 5, Martinus Nirhoff, Dordrecht, 1984.
[20] C. García Garino., A contribution to Computational Mechanics of elastoplastic solids under large deformations, Ph.D. Thesis, Univ. Politécnica de Cataluña, 1993.
[21] C. García Garino, and J. Oliver., Use of a large strain elastoplastic model for simulation of metal forming processes in: J.L. Chenot, R. Wood and O.C. Zienkiewicz (Eds.), *NUMIFORM '92*, A.A. Balkema, Rotterdam, Netherlands, 1992.
[22] C. García Garino, and J. Oliver., Simulation of a sheet metal forming processes using a frictional finite strain elastoplastic model, in: Ch. Hirsch et al. (Eds.), *Numerical Methods in Engineering 92*, Elsevier, Amsterdam, 1992.
[23] J.C. Simo, M.S. Rifai and D.D. Fox, On a stress resultant geometrically exact shell model. Part IV: Variable Thickness shell with through the thickness stretching, *Comput. Methods Appl. Mech. Engng.* 81, (1990) 91–126.
[24] J.C. Simo and J.G. Kennedy, On a stress resultant geometrically exact shell model. Part V: Nonlinear plasticity. Formulations and integrations algorithms, *Computer. Methods. Appl. Mech. Engng.*, to appear.
[25] F. Flores and E. Oñate., New shell elements for non-linear structural analysis, Research Report, CIMNE, Barcelona, (1993).